

Design, fabrication and dynamic analysis of a PZT-actuated silicon suspension

Tsung-Lin Chen and Roberto Horowitz
Computer Mechanics Laboratory
Berkeley Sensor and Actuator Center
Department of Mechanical Engineering
University of California at Berkeley, CA 94720-1740
tsunglin@me.berkeley.edu, horowitz@me.berkeley.edu

Abstract

A silicon suspension, suitable for use in a piezoelectrically actuated dual-stage servo system for magnetic Hard Disk Drives (HDDs), has been designed, fabricated and partially tested on the rotating disk. The suspension has an integrated gimbal structure and features that are useful for attaching PZT ($\text{Pb}(\text{Zr}_x\text{Ti}_{1-x})\text{O}_3$) strips. Under a 30 V applied voltage, the PZT strips stretch the suspension, producing an effective 1.3 μm magnetic head radial motion. The suspension has an in-situ piezoresistive film, which produces a signal proportional to the in-plane suspension bending. This signal can be used as an additional relative position error signal, which greatly improves the robustness of the track-following HDD servo. Micro-fabrication techniques, suitable for fabricating this high performance one-pieced silicon suspension, are also presented.

1 INTRODUCTION

The areal data density of magnetic Hard Disk Drives (HDDs) is increasing at the annual rate of more than 60%. It is well known that two of the main factors that limit further performance improvements are the friction and other nonlinearities present in the voice coil motor (VCM) ball bearings and the existence of multiple structural resonance modes in the VCM, E-block and suspension. It has been proposed that one possible solution to overcome these limitations is to incorporate a secondary actuator, which moves the magnetic head relative to the suspension, and implement a dual-stage servo [4] [2] [11] [10] [7]. This secondary actuator has to be capable of extending the dual-stage bandwidth beyond 2 KHz, in order to provide enough low frequency attenuation for friction and windage disturbances and to counteract suspension vibration induced runout.

There are many papers in the literature that report

on the design and implementation of piezoelectrically actuated suspensions as a means of dual-stage actuation (see for examples [6] [3]). In most designs, the piezoelectric actuators are placed between the E-block and the suspension, to produce a sufficiently large magnetic head motion. This arrangement is effective in designing dual-stage servo system that attain large low frequency runout attenuation, but may be susceptible to instabilities due to the excitation of suspension resonance modes.

Most dual-stage servo controllers only utilize the position error signal (PES) of the magnetic head relative to the center of data track for closed-loop track following control. These systems have a single-input-multi-output (SIMO) control architecture. However, in some instances, it is also possible to measure the relative position error signal (RPES) of the magnetic head relative to the VCM. In this case, the control architecture is multi-input-multi-output (MIMO). As shown in [7], the RPES can be used in a MIMO controller to damp out the second stage actuator's resonance mode and enhance the overall robustness of the system.

In this report, we propose a new suspension design, which allows the placement of piezoelectric (PZT) actuators on the suspension, at a location that is very close to the gimbal, while still achieving a 1 μm of magnetic head radial motion. Thus, in this configuration, the secondary actuators not only are able to attenuate low frequency runout, but also are able to partially compensate for runout induced by E-block and suspension vibration. Moreover, the design incorporates in-situ piezoresistor films, which produce a signal proportional to the deflection of the suspension when it is flexed by the PZT actuators, and can be used as the RPES in a MIMO dual-stage servo control architecture.

The field of micro-electromechanical systems (MEMS) is growing rapidly. Micromechanical structures are currently being investigated for a wide variety

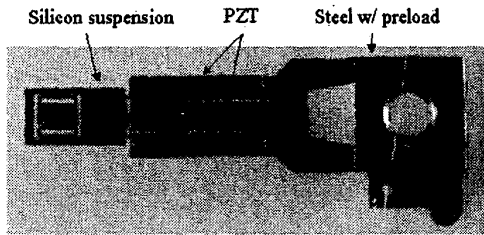


Figure 1: Prototype of PZT-actuated silicon suspension

of applications because they are generally several orders of magnitude smaller than their conventional counterparts, can easily be integrated with electronic circuits and can potentially achieve high performance with low fabrication costs. The use of silicon as the MEMS structure material has been summarized by [8]. Current deep reactive ion etch (DRIE) processes are able to achieve high aspect ratio (> 25:1) mechanical structures and make the micromachining a more promising fabrication technique for actuators as well as sensors [5]. This report also presents a microfabrication process for building a proposed one-piece silicon suspension design, which is suitable for PZT actuation, and has an integrated gimbal, an in-situ RPES sensor and electrical interconnects.

2 DESIGN OF PZT-ACTUATED SILICON SUSPENSIONS

Fig. 1 shows a photograph of our PZT-actuated silicon suspension prototype. The suspension was microfabricated using single-crystal silicon as the structure material and has an in-situ piezoresistive film (piezoresistor) deposited on it. Four pieces of bulk PZT strips are glued to the silicon suspension: one pair is glued on the top side, the other on the bottom. These PZT strips leverage in a push-pull scheme and move the magnetic head in the in-plane radial direction. When the PZT stretches the suspension to position the magnetic head, it also stretches the deposited piezoresistive film. This piezoresistor produces an electrical signal that is proportional to its deformation and can be used to determine the position of the magnetic head relative to the VCM, this signal is known as the RPES. The silicon suspension is subsequently glued to a pre-cut steel portion, as shown in the figure. This pre-cut steel suspension is pre-bent and has a pivot which is attached to the E-block. The pre-bend in the steel portion of the suspension is necessary to provide a downward pre-load force on the slider, which counteracts the air bearing forces that act on the slider when it flies on top of the rotating hard disk. The steel-silicon suspension assembly shown in Fig. 1 has the same boss-to-gimbal length

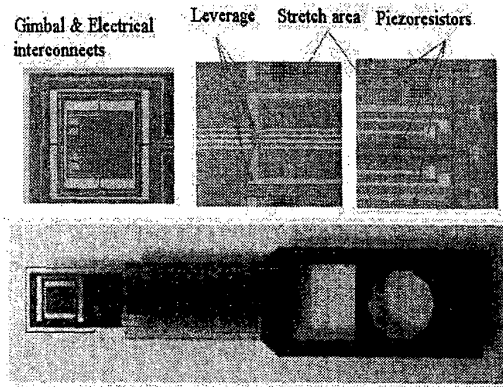


Figure 2: Features on silicon suspension

as most commercial products.

2.1 Silicon suspension

The silicon suspension design incorporates several special features for enabling PZT actuation as shown in Fig. 2. These enhance the dual-stage servo performance and lower the required PZT driving voltage. Features on the silicon suspension include: "Stretch area", "Leverage structure", "RPES sensor", "Integrated gimbal" and "Electrical interconnects". The "Stretch area" was designed to lower the driving voltage on the PZT strips while the overall suspension can still be sufficiently stiff to meet other performance requirements. The "Leverage structure" transforms the axial push-pull movement of the PZT strips into an in-plane angular motion of the integrated gimbal structure. The "RPES sensor" was facilitated by patterning the piezoresistive film that was in-situ deposited on the silicon suspension. It has high sensitivity to measure the sub-micron displacement for the magnetic head. The "Integrated gimbal" has a new torsion bar design, "double flexure", to produce the necessary pitch and roll gimbal flexibility while

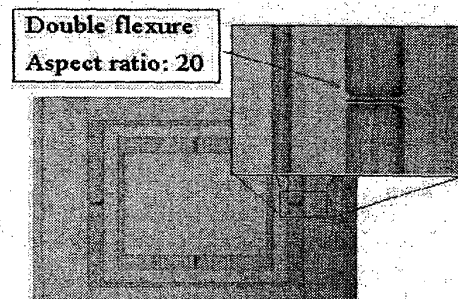


Figure 3: Silicon gimbal: flexure size 150*10*80 μm

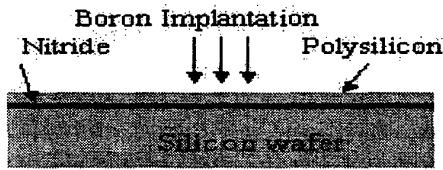


Fig. 4a. Piezoresistor layer

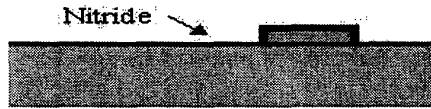


Fig. 4b. Piezoresistors patterning

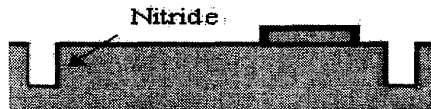


Fig. 4c. Structure patterning

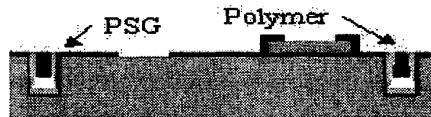


Fig. 4d. Planarization



Fig. 4e. Metallization



Fig. 4f. Release

Figure 4: Silicon suspension fabrication process flow

providing as high as possible in-plane and out-of-plane bending stiffness. A closeup of the integrated silicon gimbal structure is shown in Fig. 3. The "Electrical interconnects" transfers the electrical signals from magnetic head to the contact pads located at the end of suspension. These metal leads consist of 15 nm of chrome and 0.5 μm of copper. Details for these features can be found in our previous report [1].

2.2 Fabrication process

A simple and reliable SOI-like fabrication process has been developed for fabricating these structures. This process is compatible with most surface micromachining processes. Moreover, it produces high aspect ratio 3-dimensional structures, without requiring costly SOI wafers. The starting material is a highly

	Silicon gimbal (FEM)	TSA series	Silicon gimbal (measure)
Roll ($\mu\text{Nm/deg}$)	1.4 (1817 Hz)	0.85 -1.5	1925 Hz
Pitch ($\mu\text{Nm/deg}$)	1.16 (2088 Hz)	0.85 -1.5	1700 Hz
Sway (KHz)	11.3	6.8 -10.5	
Out-of-plane (KN/m)	11.5		

Table 1: Dynamic characteristics of silicon gimbal

conductive, double-side polished, 1-0-0 wafer. The process uses an Inductive Coupled Plasma (ICP) system to produce high aspect ratio silicon structures. In order to prevent equipment contamination, the metallization step has to be performed after the ICP deep trench etch. However, this process arrangement makes the fine lithography hard to achieve, due to the bad surface topography resulting from the deep trenches [12]. Here we have developed a new and simple planarization process to achieve high precision lithography. In this planarization process, trenches are sealed by LPCVD phospho-silicate glass (PSG) and spin-on polymer. The surface is planarized by removing polymer and PSG from the top using oxygen plasma and buffered hydrofluoric acid. After that, chrome film and copper film are evaporated on the surface and a lift-off process is subsequently performed to form the electrical interconnects. Lastly, the structures are released by a KOH backside etch. The fabrication process flow is shown in the Fig. 4.

3 RESULT AND DISCUSSION

Scanning Laser Doppler Velocimeter (LDV) and shake table were used to examine the dynamic characteristics of steel-silicon suspension. The results were compared with a commercial product (the TSA

	Silicon suspension (FEM)	TSA2030 TSA2030 TSA2030	Silicon suspension (measure)
1st Bend	20 N/m	14.7 N/m	306 Hz
2nd Bend	2402 Hz	1640 Hz	2056 Hz
1st Torsion	2638 Hz	2720 Hz	2362 Hz
2nd Torsion	7639 Hz	6500 Hz	6438 Hz
3rd Bend	4514 Hz		4487 Hz
1st Sway	10216 Hz	10900 Hz	9637 Hz

Table 2: Dynamic characteristics of steel-silicon suspension

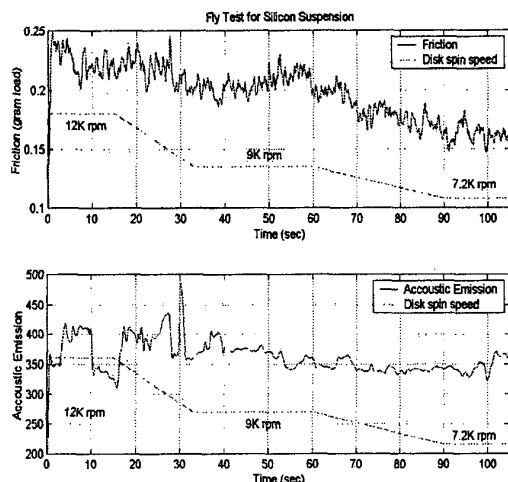


Figure 5: Fly-ability test for steel-silicon suspension

series, produced by Hutchinson Technology Inc.). FEM simulation and experimental results are both listed in Table 1 and Table 2 for comparison. The FEM analysis and LDV measurements show that the first torsional mode of the suspension is due to the steel component, which is located between the PZT strips and the E-block pivot point (see Fig. 1). This resonant mode is about 2.3 kHz and will be the first resonance encountered by the VCM section of the dual-stage servo. The 2nd torsion mode is about 6.4 kHz and is due to the two stretch areas moving up and down. The push-pull actuation scheme in this suspension design produces a small asymmetry along the out-of-plane direction, which can excite this resonant mode. Therefore, this mode is predicted to be the first resonance mode that will be encountered by the second-stage PZT component of the dual-stage servo. These arguments will be re-examined with the results from PZT actuation shown in Fig. 6. FEM simulations also predict that the maximum stress is about 0.5 Gpa, assuming that a 2 gram vertical load is acting on the picoslider. The fracture strength for micromachining single crystal silicon is reported to be between 2-7 GPa [9].

A Fly-ability test were performed with this steel-silicon suspension. The suspension was lowered onto the disk while the disk was spinning at 12000 RPM. The experiment started with disk spinning at 12000 RPM and it was slowly decelerated to 7200 RPM for the purpose of examining the friction and impact effect which may take place between the disk and the picoslider. The disk spin-speed profile can be seen in the Fig. 5. When the picoslider makes contact with the disk, the friction force will increase and the acoustic-emission signal increases. From Fig. 5, it

can be concluded that one collision took place at time of 30 sec with the indication that the acoustic emission spikes up. However, there is no obvious increase in friction at the relative location of friction plot. One possible explanation for this apparent discrepancy is that the friction signal is noisy, therefore it is difficult to distinguish a small amount in friction increase due to the slider collision with the disk, while the thrust of friction is reducing due to deceleration of the disk spin speed. More collisions should have been observed at lower disk rotation speed regime due to the reduction of fly height. We are suspecting that some dirt was trapped on the surface of picoslider, which produced a shock absorber for the collision. The torsion bars for the integrated gimbal structure remained undamaged at the friction force around 3 gram and eventually broke when the friction force reached 13 gram. This testing results suggest the necessity of utilizing a load/unload mechanism to this suspension, in order to prevent excessive friction forces which can damage the gimbal, when the HDD is turned on/off. Such mechanism are currently used by some manufactures. More fly-ability experiments are needed to evaluate the characteristics.

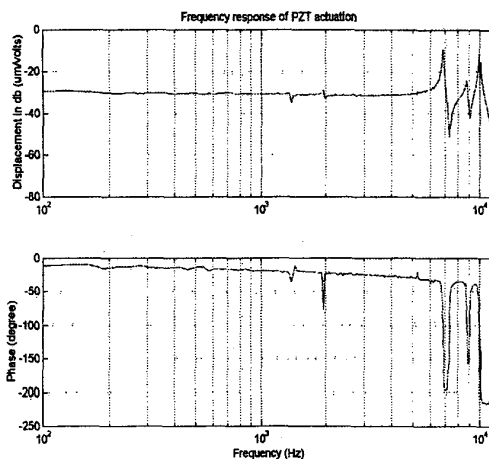


Figure 6: Frequency response of PZT actuation. The resonant frequency is 7 KHz w/ picoslider

Fig. 6 and Fig. 7 show that the PZT actuators can position the magnetic head $\pm 1.3 \mu\text{m}$ under a 2 KHz input excitation with a 30 Volt amplitude. The first structural resonant mode for PZT actuation is observed to be at about 7 KHz and the second resonance at 10 KHz. The first resonance is due to torsional motion and second resonance is due to sway motion, as indicated by their respective phase-delay shown in the lower chart of Fig. 6. At 7 KHz, the phase-delay drops and jumps right back; at 12 KHz, it drops but it does not come back right away. This experimental

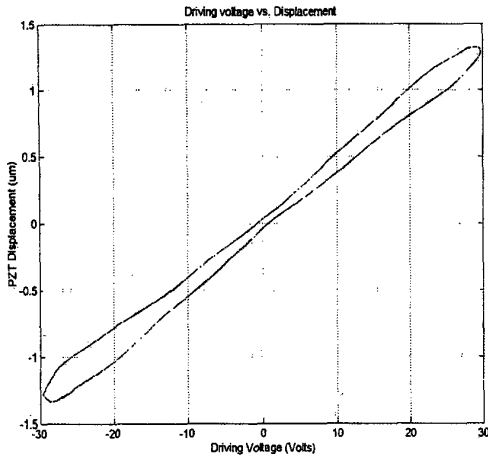


Figure 7: Characteristics of PZT actuation

result agrees with FEM/LDV testing (see Table 2). From Fig. 7, the nonlinear effect associated with PZT actuation and asymmetry from the suspension assembly is observed to have the displacement about $0.25 \mu\text{m}$.

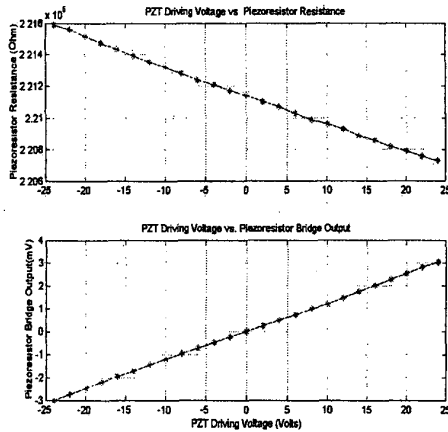


Figure 8: Characteristics of Piezoresistors

The characterization of the RPES sensors was conducted by applying an input voltage to the PZT actuators and measuring the output of the piezoresistive Wheatstone Bridge. The experimental data in Fig. 8 shows a linear response of the piezoresistor bridge. The sensitivity of this piezoresistive film is calculated to be $1.81 \text{ K}\Omega/\mu\text{m}$. It corresponds to the gauge factor of 30. The output of the Wheatstone resistor bridge is $12.13 \text{ mV}/\mu\text{m}$ under 5 V dc bias. A large feedthrough

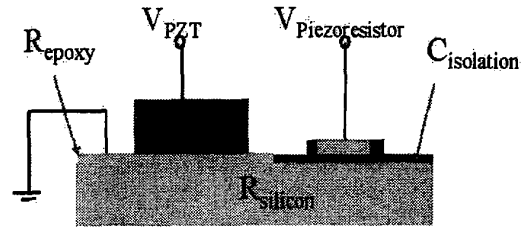


Figure 9: A resistor-capacitor schematic drawing for PZT actuated silicon suspension

from the input voltage applied to the PZT actuators to the piezoresistors RPES output was observed during the experiment. To better understand this problem, a simple resistance-capacitance circuit model was derived, as shown in Fig. 9. The analysis suggests that the feedthrough is due to the finite resistance of the epoxy used to glue the PZT strips to the silicon suspension in the stretch areas. Unfortunately, the driving voltage for PZT actuators has a magnitude in the tens of Volts, while the position-sensing signal produced by piezoresistor bridge is at the mini-volt level. Thus, the resistance of epoxy would have to be in the milli-ohm level, in order to meet the SNR (signal-noise-ratio) specification for RPES. This suggests that using a more conductive epoxy than the one used to assemble the prototype will not solve this problem completely. Another solution to the feedthrough problem is to use a frequency modulation technique in this piezoresistors bridge. A simple frequency modulation scheme was successfully implemented and the results are shown in Fig. 10.

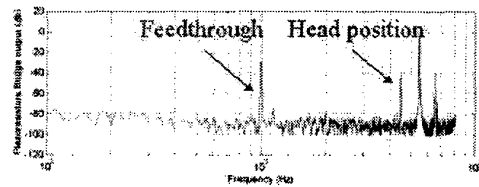
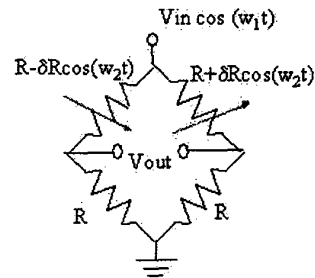


Figure 10: Modulation for the piezoresistors sensing bridge

4 CONCLUSION

A one-pieced silicon suspension was designed, fabricated and tested, which can be flexed by piezoelectric PZT strips and used as a second-stage actuator in a dual-stage servo system. The PZT actuation is able to drive the magnetic head $\pm 1.3 \mu\text{m}$ with ± 30 Volts applied on the PZT strips. The suspension also has an integrated gimbal structure. The first resonance frequency for PZT actuation is about 7 KHz. The dynamic response of this suspension measured by scanning LDV is similar to that of commercially available steel suspensions. This silicon suspension has been flown on the rotating disk. Structures are intact with applying force from out-of-plane pre-load and in-plane friction between spinning disk and picoslider under normal operating condition. However, a slider load/unload mechanism, which is commonly used by some manufacturers must be used to prevent the torsion bars from fracturing under excessive friction forces when the HDD is turned on/off. More experiments are needed to evaluate the fly characteristics. The implemented piezoresistive RPES sensing scheme has a fairly linear response and a high sensitivity (Gauge Factor). A large feedthrough from driving signal to sensing signal has been observed. It was attributed to the small electrical resistance of the conductive epoxy that was used to glue the PZT strips to the silicon structure. The use of a higher conductivity epoxy will not significantly alleviate this problem, due to the 80 dB magnitude difference between the driving and sensing signals. An alternative solution to the feedthrough problem is to apply a frequency modulation technique to the sensing scheme proved to be feasible. The feasibility of frequency modulation was demonstrated by the experimental data.

5 Acknowledgment

This work was supported by a DARPA grant and the Computer Mechanics Laboratory. The authors wish to thank Brian Thornton in helping with the fly-ability test and the LDV dynamic characterization of the suspension.

References

- [1] Chen, Tsung-Lin, Horowitz, Roberto. (2000) Design and Fabrication of PZT-Actuated Silicon Suspensions, *IEEE Mechatronics 2000*, Atlanta, Georgia, 6th-8th Sept.
- [2] Cheung, P., Horowitz, R. and Howe, R. (1996).

Design, Fabrication, Position Sensing and Control of an Electrostatically-driven Polysilicon Microactuator. *IEEE Transactions on Magnetics*, Vol. 32, No. 1, pp 122-128.

- [3] Evans, R. B., Griesbach, J. S. and Messner, W. C. (1999). Piezoelectric Microactuator for Dual Stage Control. *IEEE Trans. on Magnetics*, Vol. 35 No. 2, pp 977-982.

- [4] Fan, L. S., Ottesen, H. H., Reiley, T. C. and Wood, R. W. (1995). Magnetic Recording Head Positioning at Very High Track Densities Using a Microactuator-based Two-stage Servo System. *IEEE Trans. on Industrial Electronics*, Vol, 42, No. 3, pp 222-233.

- [5] Kuhl, Karl, Vogel, Stefan Schaber, Ulrich, Schafflik, Rainer and Hillerich, Bernd (1998). Advanced Silicon Trench Etching in MEMS Applications. *SPIE Conference on Micromachining and Microfabrication Process*. Vol. 3511, pp 97-105.

- [6] Mori, K., Munemoto, T., Otsuki, H., Yamaguchi, Y., Akagi, K. (1991). A Dual-Stage Magnetic Disk Drive Actuator Using a Piezoelectric Device for a High Track Density. *IEEE Trans. on Magnetics*. Vol. 27, No. 6, pp 5298-5300.

- [7] Li, Y. and Horowitz, R. (2000). Track-Following Controller Design of MEMS Based Dual-Stage Servos in Magnetic Hard Disk Drives. *International Conference on Robotics and Automations*. April, 2000. San Francisco, USA.

- [8] Peterson, Kurt E. (1982). Silicon as a Mechanical Material. *Proceedings of the IEEE*, Vol. 70, No. 5, pp 420-457.

- [9] Peason, G. L., Read, W. T. and Feldmann, W. L. (1957). Deformation and Fracture of Small Silicon Crystals. *ACTA METALLURGICA*, Vol. 5, April, pp 181-191.

- [10] Roberto Oboe, A. B. and Murari, B. (1999). Modelling and Control of a dual stage actuator hard disk drive with piezoelectric secondary actuator. *International Conference on Advanced Intelligent Mechatronics*, September, Atlanta, USA, pp 138-143.

- [11] Takaishi, K., Imamura, T. Mizoshita, Y., Hasegawa, S., Ueno, T. and Yamada, T. (1996). Microactuator Control For Disk Drive. *IEEE Transaction on Magnetics*, Vol. 32, No. 3, pp 1863-1866.

- [12] Yoon, Jun-Bo, Oh, Gilbert Y., Han, Chul-Hi, Yoon, Euisik and Kim, Choong-Ki (1998). Planarization and trench filling on severe surface topography with thick photoresist for MEMS. *SPIE Conference on Micromachining and Microfabrication Process Technology*, Vol. 3511, pp 297-306.